Modeling of Tapered Anechoic Chambers

Zubiao Xiong, Zhong Chen
RF Engineering
ETS-Lindgren, Inc.
Cedar Park, TX, USA
Zubiao.Xiong@ets-lindgren.com

***Abstract*—A hybrid method that combines the finite element method (FEM), the Floquet mode analysis and the shooting and bouncing ray method (SBR) is presented to solve the quiet-zone field in large tapered anechoic chambers. In the method, the field equivalence principle is employed to replace the throat of the tapered chamber by a set of equivalent electric and magnetic currents. The Floquet mode analysis is employed to approximate the rest of the absorber lined walls by virtual surfaces with equivalent reflection coefficients. The total quiet-zone field then becomes the superposition of the field radiated by the equivalent currents, and the field scattered by the virtual reflective surfaces. The scattered field is calculated from the SBR method. The required equivalent currents of the throat and the reflection coefficients of absorber array walls are computed with the use of the FEM, which allows the considerations of the complex structure and near-field interaction. Numerical examples are presented to demonstrate the feasibility of the proposed method.**

I. Introduction

The tapered anechoic chamber can offer better performance than the standard rectangular chamber for antenna measurements at lower frequencies. The feed antenna is placed at the throat of a tapered chamber to reduce the phase differences among the direct wave and the reflected waves. Therefore, a smother illumination amplitude in the target region can be achieved [1], [2].

Although the tapered chamber has been developed for more than 50 years, a thorough performance analysis through computer simulation is still challenging. Full-wave solvers are usually not applicable due to the large electrical size. Ray tracing technique [3] such as SBR method [4] is widely used in the industry [5]. However, it does not provide enough accuracy at frequencies below 500 MHz. The antenna becomes physically large at low frequencies. Besides, it is desired to place the source antenna as close as possible to the apex of the tapered section, which makes the antenna very close to absorber walls. In such cases, the ray approximation starts breaking down. More complex wave phenomenon must be taken into account. Lacking an accurate model for low frequencies becomes a major obstacle for tapered chamber design and prediction.

A novel algorithm is presented in this paper, which overcomes the accuracy problem in ray trace method with minimum increase in computing time and resources. The algorithm separate the whole chamber into two decoupled parts: a small throat part solved with the FEM method, and the rest of the chamber solved with the SBR method. The equivalent surface currents on the interface from the FEM domain solution are used as equivalent sources to the SBR domain. We then approximate absorber arrays as flat surfaces through Floquet mode expansion. The chamber model is simplified by applying the approximation to all the absorbers lined walls within the SBR domain. Comparison against full-wave simulations demonstrates its excellent accuracy and efficiency.

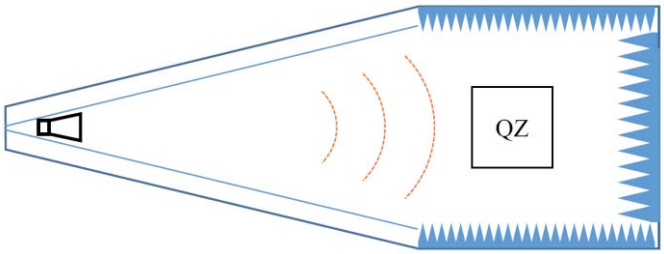

Figure 1. Illustration of a tapered anechoic chamber with absorbers.

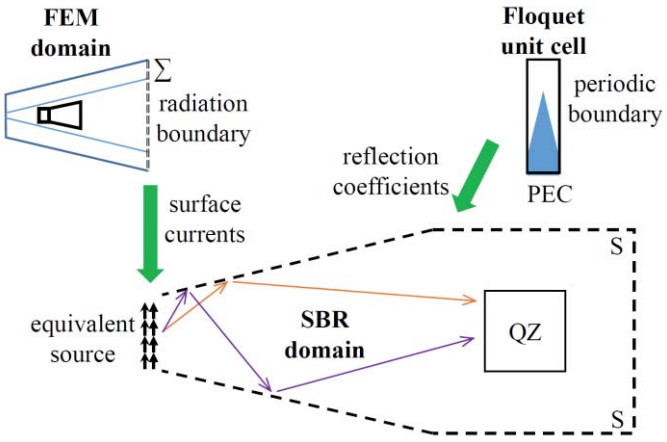

Figure 2. Hybrid FEM/Floquet Modes/SBR technique for simulating tapered anechoic chambers.

II. Methodology

Because the source antenna is in close proximity to the absorbers near the apex, as shown in Figure 1. , high frequency techniques can not be applied directly for simulating the tapered anechoic chamber. The idea proposed in this paper is to divide the whole chamber into two parts: the throat of the

tapered section including the source antenna, and the rest of the chamber. The throat is simulated by using the FEM, with a radiation boundary condition on the interface. Then the surface currents on the interface are extracted and fed as the equivalent source to the SBR domain. Since the waves mostly propagates from the throat towards the designated quiet zone (QZ), it is not necessary to take into account the backward interaction from the SBR domain to the FEM domain. The absorber arrays on the chamber walls are analyzed by using the Floquet modal expansion. The resulting reflection coefficients of Floquet modes will be used by the SBR simulation. Figure 2. shows the process graphically of applying the hybrid FEM/Floquet Modes/SBR technique.

A. FEM Modeling of the Throat of the Tapered Section

The FEM domain shall conclude the part of the tapered section of the chamber, which strongly couples with the source antenna. By applying a radiation boundary condition on the interface $\sum$ between the FEM domain and the SBR domain, the fields within the FEM domain can be solved with commercial FEM solvers. We take the equivalent surface currents on the interface as

$$\bar{J}_\Sigma = \hat{n}_\Sigma \times \bar{H}_\Sigma ,\ \bar{M}_\Sigma = \bar{E}_\Sigma \times \hat{n}_\Sigma , \tag{1}$$

where $\hat{n}_\Sigma$ is the outward normal vector of the interface, $\bar{E}_\Sigma$ and $\bar{H}_\Sigma$ are the electric and magnetic fields on the interface, respectively. According to the surface equivalence principle, the FEM domain now can be substituted by the equivalent sources $\bar{J}_\Sigma$ and $\bar{M}_\Sigma$.

B. Floquet Modal Analysis of Periodic Absorber Arrays

For an infinite doubly periodic absorber array (on *xy* plane), the scattered field propagates towards the following directions:

$$\theta_{scat} = \arccos\left(k_z/k_0\right),\ \phi_{scat} = \arctan2\left(k_y, k_x\right), \tag{2}$$

where k_x , k_y and k_z are the *x*, *y* and *z* components of the wave vector

$$\begin{aligned} k_x &= -k_0 \sin\theta_{inc}\cos\phi_{inc} + 2\pi m/D_x \\ k_y &= -k_0 \sin\theta_{inc}\sin\phi_{inc} + 2\pi n/D_y \\ k_z &= \sqrt{k_0^2 - k_x^2 - k_y^2} \end{aligned} , \tag{3}$$

where k_0 is the wavenumber in free space, θ_{inc} and ϕ_{inc} denote the incident angles of the impinging wave, D_x and D_y are the inter-element spacing along *x* and *y* directions, and (*m*, *n*) represents the indexes of the Floquet modes. It is evident from (3) that all higher order Floquet modes other than the two fundamental modes are evanescent, if D_x and D_y (which represent the spacing between the periodic absorbers) are smaller than half a wavelength. Absorbers in the tapered chamber usually do not exceed 12-inch periodicity. For the spacing of 12 inches, the first higher-order propagating modes starts at 492 MHz. On the back wall, large absorbers longer than 60 inch may be used, which can be 24 inch wide. High order modes are possible at lower frequencies. However, the incident field coming from the throat impinges on the back wall with small incident angles, which means they can only produce propagating modes at large scattering angles. Those scattered waves are unlikely to enter into the quiet zone. They can be neglected. Therefore, for the frequencies ranging from 100 MHz to 500 MHz, which are under consideration in the paper, we assume that only the two fundamental modes propagate in the chamber.

The S-parameters of the two fundamental Floquet modes represent the specular reflection coefficients of the corresponding absorber array in TE and TM polarizations, respectively. They can be obtained by solving a unit cell in the FEM method. The Floquet port and the periodic boundary conditions are applied to the unit cell. Equivalently, the Floquet port can be achieved by a plane wave excitation with a perfect matched layer (PML) boundary condition above the structure.

C. Hybridization with SBR technique

Each absorber wall in the SBR domain is replaced by a virtual surface with equivalent reflection coefficients. Instead of tracing rays into each piece of absorbers, the rays are bounced by the flat surfaces. This reduces the simulation complexity drastically, which paradoxically may be more accurate because the absorbers are electrically small in the low frequency range of interest. The electromagnetic waves do not see the microstructures.

For every ray bounce having an incident ray and a corresponding reflected ray, the total field is the summation of the incident field and the reflected field. According to surface equivalence principle, the equivalent surface currents are

$$\bar{J}_S = \hat{n}_S \times (1 + \bar{\bar{\Gamma}}_H)\bar{H}_i ,\ \bar{M}_S = (1 + \bar{\bar{\Gamma}}_E)\bar{E}_i \times \hat{n}_S , \tag{4}$$

where $\hat{n}_S$ is the normal vector of the bouncing surface, $\bar{\bar{\Gamma}}_E$ and $\bar{\bar{\Gamma}}_H$ are the dyadic reflection coefficients for E field and H field obtained from section II.B, respectively.

The total field in the quiet zone will be the summation of the incident field generated by the equivalent sources $\bar{J}_\Sigma$ and $\bar{M}_\Sigma$, and the scattered field generated by the equivalent SBR surface currents $\bar{J}_S$ and $\bar{M}_S$:

$$\bar{E}_{tot} = \bar{E}_i + \bar{E}_{sc} ,\ \bar{H}_{tot} = \bar{H}_i + \bar{H}_{sc} , \tag{5}$$

where

$$\bar{E}_{i,sc}(\bar{r}) = \int_{\Sigma,S} \bar{M}_{\Sigma,S}(\bar{r}') \times \nabla g(\bar{r} - \bar{r}') ds' - j\omega\mu_0 \int_{\Sigma,S} \left(\bar{\bar{I}} + \frac{\nabla\nabla}{k_0^2} \right) g(\bar{r} - \bar{r}') \cdot \bar{J}_{\Sigma,S}(\bar{r}') ds'$$

$$\bar{H}_{i,sc}(\bar{r}) = -\int_{\Sigma,S} \bar{J}_{\Sigma,S}(\bar{r}') \times \nabla g(\bar{r} - \bar{r}') ds' - j\omega\varepsilon_0 \int_{\Sigma,S} \left(\bar{\bar{I}} + \frac{\nabla\nabla}{k_0^2} \right) g(\bar{r} - \bar{r}') \cdot \bar{M}_{\Sigma,S}(\bar{r}') ds' \quad (6)$$

where ε_0 and μ_0 are the permittivity and the permeability in vacuum, ω is the angular frequency, $\bar{\bar{I}}$ is the unit dyadic, and $g(\bar{R})$ is the Green's function in free space

$$g(\bar{R}) = \frac{e^{-jk_0 R}}{4\pi R}, \quad (7)$$

III. Numerical Results

The proposed method has been validated by comparing it against a full-wave simulation with ANSYS HFSS. The chamber used in the comparison is 54-meter long in total composed by a 42-meter long tapered section and a rectangular section of 12-meter side. The quiet zone is 4-meter large centered in the rectangular section. The back wall behind the quiet zone is lined with 72 inch long pyramidal absorbers. The side walls, ceiling and floor are lined with 36 inch long pyramidal absorbers.

Firstly, the full chamber was solved by using the HFSS FEM solver from 50 MHz to 300 MHz with a step of 50 MHz. Since the chamber is symmetrical around its longitudinal axis, two symmetric boundary conditions were applied to reduce the problem domain to a quarter. This solution is as the reference for the following comparisons. For the hybrid method, we used HFSS to solve a 12-meter long throat and the unit cell for each type of absorber firstly, and then utilized an in-house SBR code to solve the quiet-zone field. In the SBR simulation, 4 bounces were chosen to terminate the rays. Figure 3. shows the electric field distribution on the horizontal plane (z=0) within the quiet zone. Due to the limited space, only results for 100 MHz, 200 MHz and 300 MHz are shown. The values shown in Figure 3. are normalized to the maximum within the plotting area. The color scale is from blue (-2 dB) to yellow (0 dB). As can be seen, the hybrid method can predict the quiet-zone field very well. Two important phenomenon, the longitudinal ripple caused by the back wall reflections, and the transverse amplitude tapering caused by the tapered section, can be identified easily just as in the full chamber FEM solution. The small discrepancy could be caused by not taking into account the diffractions on the edges of absorber walls in the SBR calculation. It will be investigated in future studies.

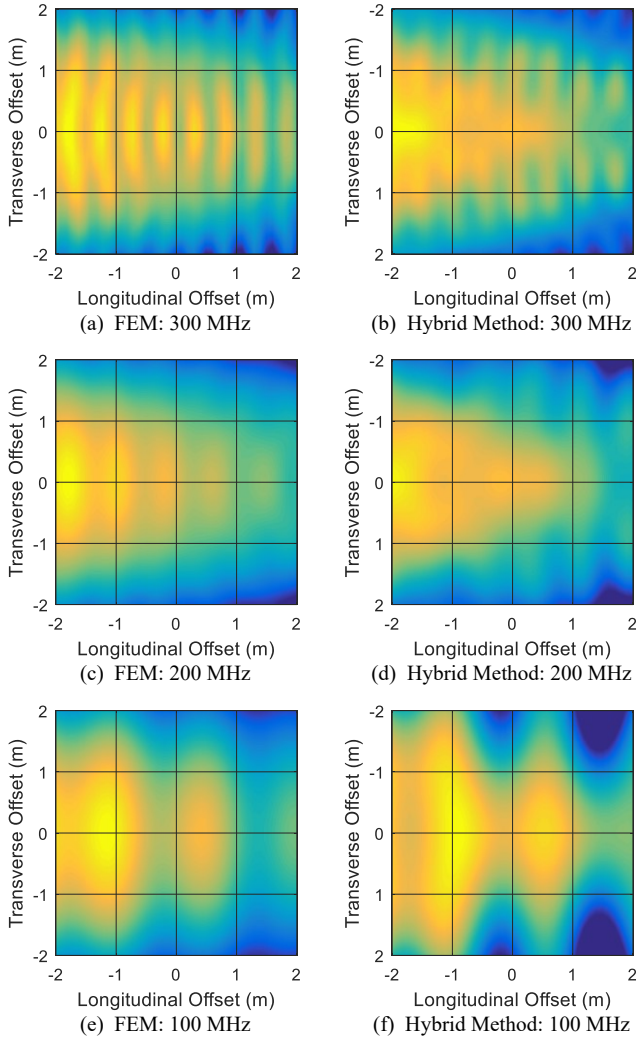

Figure 3. Electric field on the horizontal plane (z=0) within the quiet zone. The values are normalized to the maximum and plotted in dB scale. The color scale is from blue (-2 dB) to yellow (0 dB).

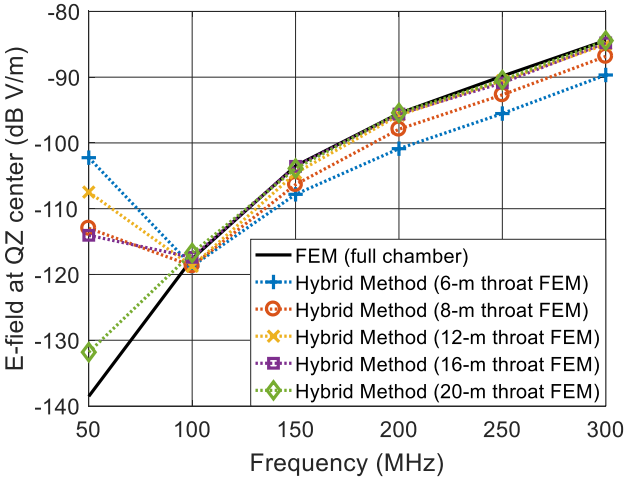

Figure 4. Electric field strength at the quiet zone center.

The selection of the size of the throat FEM domain is important to the accuracy and efficiency of the hybrid method. In order to investigate its influence, we simulated various throat lengths ranging from 6 meter to 20 meter. Figure 4. shows the electric field strength at the quiet zone center point for different frequencies. It can be seen that the hybrid method solution converges to the full chamber FEM solution as the length of the throat domain increases. For frequencies above 100 MHz, 12-meter throat is sufficient. However, a much longer throat is needed below 100MHz.

We summary the CPU time and the memory usage of computation for simulating the tapered chamber in Table I. All calculations were performed using 32 cores in a Windows server with 2.2 GHz Intel Xeon E5-4620 CPUs and 1 terabyte RAM. In this example, the hybrid method is 6 times faster and needs much less memory space than the FEM-only simulation. Actually, the symmetric boundaries used in the FEM-only simulation significantly reduced its CPU time and memory requirement. For cases that the chamber is not symmetric, the FEM-only simulation may not be even feasible. The hybrid method might be the only choice.

TABLE I. THE CPU TIME AND MEMORY REQUIREMENT OF COMPUTATION OF A 54-METER LONG TAPERED ANECHOIC CHAMBER.

		CPU	**Memory**
FEM method (full chamber)		9.5 hours	640 GB
Hybrid method (using 12-m throat)	FEM (unit cells) [a]	50 minutes	2.0 GB
	FEM (throat)	23 minutes	37.5 GB
	SBR	1.2 hours	1.5 GB
	total	1.6 hours	37.5 GB

[a]The unit cells are solved only once and the solutions can be reused in different chamber simulations. Therefore, the total CPU time and memory usage of the chamber simulation do not include that of unit cell simulations.

IV. CONCLUSION

In this paper, a hybrid FEM/Floquet Modes/SBR technique has been applied to analyze the quiet-zone field for large tapered anechoic chambers. We first employ the field equivalence principle to replace the chamber throat by a set of equivalent electric and magnetic currents. We then use the FEM method to compute the equivalent currents and the SBR method to calculate the field scattered by the large chamber body without the throat. Numerical examples are presented, demonstrating that the tapered chamber problem can be accurately, efficiently computed using this technique.

REFERENCES

[1] L. H. Hemming, *Electromagnetic Anechoic Chambers: A Fundamental Design and Specification Guide*. Piscataway, NJ: IEEE Press, 2002.

[2] H. E. King, F. I. Shimabukuro, and J. L. Wong, "Characteristics of a Tapered Anechoic Chamber," *IEEE Trans. Antennas Propag.*, vol. AP-15, no. 3, pp. 488–490, 1967.

[3] W. Fan, I. Carton, P. Kyosti, and G. F. Pedersen, "Emulating Ray-Tracing Channels in Multiprobe Anechoic Chamber Setups for Virtual Drive Testing," *IEEE Trans. Antennas Propag.*, vol. 64, no. 2, pp. 730–739, 2016.

[4] H. Ling, R.-C. Chou, and S.-W. Lee, "Shooting and bouncing rays: Calculating the RCS of an arbitrarily shaped cavity," *IEEE Trans. Antennas Propag.*, vol. 37, no. 2, pp. 194–205, 1989.

[5] Z. Xiong, J. Chen, and Z. Chen, "Low frequency modeling for electromagnetic analysis of arbitrary anechoic chambers," in *IEEE International Symposium on Electromagnetic Compatibility*, 2016, pp. 13–18.